國立交通大學

生物科技學系

碩士論文

開發奈米鑽石連結紫杉醇作爲藥物運送與癌症治療

Development of nanodiamond-conjugated paclitaxel for drug delivery and cancer therapy

研究生: 王繼慶

指導教授: 趙瑞益

中 華 民 國 九 十 九 年 七 月

開發奈米鑽石連結紫杉醇作爲藥物運送與癌症治療

Development of nanodiamond-conjugated paclitaxel for drug delivery and cancer therapy

研究生: 王繼慶　　Student: Chi-Ching Wang

指導教授: 趙瑞益　Advisor: Prof. Jui-I Chao

國 立 交 通 大 學

生物科技學系

碩 士 論 文

A Thesis
Submitted to Department of Biological Science and Technology
College of Biological Science and Technology
National Chiao Tung University
in partial Fulfillment of the Requirements
for the Degree of
Master
In

Biological Science and Technology

July 2010

Hsinchu, Taiwan, Republic of China

中華民國九十九年七月

致 謝

兩年的碩士研究生活，在一轉眼間就過了，而這篇論文的完成，要感謝許多幫助過我的人，首先要感謝我的指導教授趙瑞益教授，感謝老師這兩年來悉心的指導與關照，在撰寫論文期間，謝謝老師不辭辛勞的幫我校正與定稿。在研究所的日子哩，實驗室就像是第二個家，實驗室的夥伴們都是幫助我成長的人。我要感謝惠芳學姐和光凱學長，每當我在實驗遇到困難時，總是不厭其煩的替我找出問題，也耐心的幫助我解決口試及生活上的問題，讓我覺得能夠認識學長姐你們，是我研究所中最重要的收穫。已畢業的真宜學姐和瑞良學長，感謝你們在我碩一時的幫助及照顧。還有厚巽、靜宜、勝壹、同屆的夥伴們，互相的體諒與幫助完成這兩年的學業。實驗室的學弟妹們，芷漪、淳如、佩萱、毓婷、昱耀、旻翰，有你們的陪伴，讓我的研究所生活更加精采。最後，我要感謝我的家人，謝謝爸爸、媽媽對我的付出，給我莫大的支持，弟弟總是鼓勵與幫助我解決生活上雜事。最後我要感謝曾經幫助過我的師長與朋友們，謝謝你們。

Table of contents

page

中文摘要

利用奈米物質攜帶抗癌藥物，提供一個嶄新的機會作爲癌症的治療。在本篇研究中，我們利用一種由碳所組成的奈米材料，稱作奈米鑽石，以共價鍵的方式連結紫杉醇，作爲藥物的運送和癌症的治療。透過一連串化學修飾的合成方法，將紫杉醇鍵結到奈米鑽石的表面。在濃度 0.1-50 μg/mL 的奈米鑽石-紫杉醇處理 A549 人類肺癌細胞 48 小時之後，明顯降低癌細胞的存活率，然而單獨處理奈米鑽石或是經強鹼處理過後的奈米鑽石-紫杉醇，並不會誘發 A549 肺癌細胞的死亡。由共軛焦顯微鏡觀察，我們發現奈米鑽石-紫杉醇會進入 A549 肺癌細胞，並且位在細胞質及微小管。奈米鑽石-紫杉醇仍然具有紫杉醇的抗癌活性，會造成細胞的有絲分裂停止和細胞凋亡，並且抑制 CDC2、磷酸化 CDC2 及 cyclin B1 蛋白的表達。此外，在異體移植人類肺癌細胞到先天免疫不全的老鼠之動物實驗中，奈米鑽石-紫杉醇會抑制老鼠體內腫瘤的形成。再者，我們也發現奈米鑽石-紫杉醇在其他種類的人類癌細胞，包括大腸癌細胞(ROK 和 HCT116)和膀胱癌細胞(BFTC 905)也會誘發細胞毒性和細胞凋亡，並且造成 caspase-3 蛋白的活化及 PARP 蛋白被切割。綜合以上結果，我們已經開發出一種功能性之共價鍵結奈米鑽石-紫杉醇，具有促使有絲分裂停止、誘發細胞凋亡及抑制腫瘤形成的抗癌活性。

Abstract

Nanoparticle-conjugated anticancer drugs provide novel opportunities for cancer therapy. In this study, we evaluated nanodiamond (ND), a carbon nanomaterial, to covalently bind paclitaxel for drug delivery and cancer therapy. Paclitaxel was bound to the ND's surface through a succession of chemical modification. Treatment with 0.1-50 μg/mL ND-paclitaxel for 48h significantly reduced the cell viability in A549 human lung cancer cells. However, ND alone or denatured ND-paclitaxel (after treatment with strong alkaline solution, 1M NaOH) did not induce the damage effects on A549 cells. The ND-paclitaxel was taken into cell and located in the microtubules and cytoplasm of A549 cells observed by confocal microscopy. Moreover, ND-paclitaxel still reserves the anticancer activity of paclitaxel. ND-paclitaxel was attributed both mitotic blockage and apoptotic induction in cancer cells. The protein levels of CDC2, phosphorylated CDC2, and cyclin B1 were decreased by treatment with ND-paclitaxel. Besides, ND-paclitaxel inhibited the tumorigenesis of xenograft human lung tumor in SCID mice. Moreover, we also found ND-paclitaxel was significantly induced cytotoxicity and apoptosis in other cancer cells including colon cancer cells (RKO and HCT116) and bladder cancer cells (BFTC 905). ND-paclitaxel induced the caspase-3 activation and the protein cleavage of PARP. In summary, we have developed a functional covalent ND-paclitaxel, which still preserves its anticancer activities on the mitotic blockage, apoptosis induction and anti-tumorigenesis.

List of figures

page

Abbreviations

ND	nanadiamond
PARP	anti-poly(ADP-ribose) polymerase
DMSO	dimethyl sulfoxide
PI	propidium iodide
PBS	phosphate buffered saline
SDS	sodium dodecyl sulfate
CDKs	cyclin-dependent kinases
CDC2	cell division control protein 2
FBS	fetal bovine serum
Caspase-3	cysteine-aspartic acid protease
MTT	3-(4,5-dimethyl-thiazol-2-yl) 2,5-diphenyl tetrazolium bromide
PTX	paclitaxel
THF	tetrahydrofuran
FITC	fluorescein isothiocyanate
THP	tetrahydropyran

1. Introduction

Cancers have been become the leading reason of death in the world. In Taiwan, lung cancer has become the first mortality among all cancer patients (Department of health, Executive Yuan, 2009). Although treatments of cancers include surgery, radiation, and chemotherapy, patients in late stage diseases are usually managed primarily with chemotherapy. However, poor intracellular uptake, limited circulation stability, and normal cell damages reduce the abilities of chemotherapeutic drugs. Therefore, development of novel strategies for cancer therapy is highly desired. Nanoparticles have been evaluated for biomedical applications in recent years. Moreover, nanoparticles can be developed for biomedical application such as cancer detection and drug delivery (Kang et al., 2010; Liu et al., 2008).

Nanoparticles refer to are the substance of investigation size at range 1-100 nm at one dimension (McNeil, 2005). Nanomaterials as drug delivery systems facilitate approach for cancer therapy (Alexis et al., 2010). Nanoparticles can improve cancer therapeutics by conjugated with drugs and biological molecules (Akerman et al., 2002; Gao et al., 2004; Michalet et al., 2005; Tada et al., 2007). For example, quantum dots, which exhibit varying colors of fluorescence, have been applied for the labeling and imaging of tumors by conjugation with specific target proteins

(Akerman et al., 2002; Gao et al., 2004; Tada et al., 2007). Nanoliposomal carrying cancer drugs have been successfully used in cancer therapy, demonstrating benefits of prolonged tissue residence and reduced toxicity (Chau et al., 2006; Koshkina et al., 2003; Noble et al., 2006). Utilization liposome-encapsulated doxorubicin have been successfully used in cancer therapy, demonstrating doxorubicin displayed less cardiac toxicity (Batist et al., 2001). Besides, carbon nanotube has been used as a carrier for cancer drug delivery that effectively inhibited tumor growth in mice (Liu et al., 2008).

It has been concerned on the issue of toxic potential of nanomaterials (Nel et al., 2006; Service, 2004), although it is intensively developed for biomedical applications. A non-toxic and biocompatible nanomaterial is desired for clinical applications. Nanodiamond (ND) is a carbon derivative nanomaterial, which has been evaluated for biomedical applications in recent years. It has been shown that ND do not induce cytotoxicity in a variety of cells including lung (Liu et al., 2007; Liu et al., 2009), neuronal (Schrand et al., 2007), renal (Lechleitner et al., 2008; Yu et al., 2005), and cervical cells (Chang et al., 2008). Moreover, ND particles did not alter cell division and differentiation (Liu et al., 2009). In addition, the intravenous injection of ND particles into mice did not significantly induce symptoms of abnormality (Yuan et al., 2009). It is a relative safe nanomaterial based on its

non-cytotoxicity and biocompatibility, although ND should be to further evaluation before clinical use.

The surface of ND particles has a unique platform for conjugation of chemicals and bio-molecules after functional modifications (Yang et al., 2002; Chao et al., 2007; Ushizawa et al., 2002; Huang et al., 2004; Cheng et al., 2007; Krueger et al., 2008). ND is suitable for bioconjugation either chemically (covalently or noncovalently) or physically (adsorption) (Cheng et al., 2005; Krueger, 2008). The modified ND's surfaces have been shown to conjugate with DNA (Yang et al., 2002; Ushizawa et al., 2002), lysozyme (Chao et al., 2007), cytochrome c (Huang et al., 2004), growth hormone (Cheng et al., 2007), biotin (Krueger et al., 2008), alpha-bungarotoxin (Liu et al., 2008), and insulin (Shimkunas et al., 2009), and folate (Zhang et al., 2009). Lysozyme and alpha-bungarotoxin proteins can be absorbed on the surface of carboxylated ND via non-covalent bonding that still preserve the biological activities of these proteins (Chao et al., 2007; Liu et al., 2008). The hydrogel of ND with chemotherapeutic drugs such as doxorubicin was developed for drug delivery by non-covalent adsorption (Huang et al.,2007). In addition, ND has been covalently linked to folate for targeting cancer cells (Zhang et al., 2009).

Until now, the covalent linking of cancer drugs to ND particles and the

anticancer activities of these conjugates are poorly understood. Paclitaxel is the one of most widely used chemotherapeutic drugs in the clinic for the treatment of advanced solid carcinomas (Wang et al., 2009). Paclitaxel disturbs microtubule dynamics and impairs the transition of cells in mitosis, and leading to cell death (Wang et al., 2010).

In this study, we create a novel covalent bonded ND-paclitaxel for drug delivery and cancer therapy. ND-paclitaxel can be taken into human lung and colon carcinoma cells. More importantly, ND-paclitaxel displays anticancer activities by inducing mitotic arrest, apoptosis and anti-tumorigenesis. Accordingly, we create a functional covalent conjugation of ND and paclitaxel, which provides the possible biomedical applications for drug delivery and cancer therapy.

2. Materials and methods

2.1 Reagents and antibodies

Paclitaxel was purchased from Tokyo Chemical Industry Co. (Ltd. Japan). Powdered ND particles with diameters of 3-5 nm were purchased from Nanostructured and Amorphous Materials Inc. (Houston, TX). 3-(4,5-dimethyl-thiazol-2-yl) 2,5-diphenyl tetrazolium bromide (MTT), Hoechst 33258, and the Cy3-labeled mouse anti-β-tubulin (c-4585) were purchased from Sigma Chemical Co. (St Louis, Mo.). Anti-CDC2, anti-phospho-CDC2 (tyrsion-15, threonine-14, and threonine-161), and anti-poly(ADP-ribose) polymerase (PARP) antibodies were purchased from Cell Signaling Technology Inc. (Beverly, MA). Anti-caspase-3 antibody was purchased from BioVision (BioVision, Inc., USA). Anti-cyclin B1 (Ab-2) antibody was purchased from Oncogene Sciences (Cambridge, MA). Anti-actin (I-19) antibody was purchased from Santa Cruz Biotechnology, Inc. (Santa Cruz, CA).

2.2 Cell lines

A549 cell line (ATCC number: CCL-185) was derived from the lung adenocarcinoma. RKO (ATCC number: CRL-2677) was a colon carcinoma cell line. HCT116 (ATCC number: CCL-247) was a colon carcinoma cell line. BFTC 905 cells (BCRC number: 60068) were derived from human bladder papillary

transitional cell carcinoma.

2.3 Cell culture

A549 and BFTC 905 cells were maintained in RPMI-1640 medium (Invitrogen Co., Carlsbad, CA). RKO cells were cultured in DMEM medium (Invitrogen). HCT116 cells were maintained in McCoy's 5A medium. The complete media were supplemented with 10% FBS, 100 units/ml penicillin, and 100 μg/ml streptomycin. These cells were cultured at 37 ℃ and 5% CO2 in a humidified incubator (Thermo, Forma Scientific, Inc., Marietta, OH).

2.4 Synthesis of ND-conjugated paclitaxel

ND-paclitaxel was synthesized and kindly provided by our collaborator Dr. Chinpiao Chen (Department of Chemistry, National Dong-Hwa University, Hualien). The chemical synthetic procedure for the conjugation of ND and paclitaxel was been shown in Scheme 1. Initial chemical treatment of ND powders **(1)** by carboxylation was carried out according to standard procedure. The ND particles were stirred in a 3:1 (v/v) mixture of concentrated HCl and HNO_3 at room temperature for three days, then diluted with deionized H_2O and separated by centrifugation at 900 rpm. After centrifugation, the pellets were extensively rinsed with deionized H_2O three times. Thereafter, ND particles were heated in 0.1 M NaOH solution at 90 ℃ for 2 h. The ND particles were again heated in 0.1 M HCl at

90 ℃ for 2 h. The resulting carboxylated-ND **(2)** was dried under vacuum for 24 h. A mixture of ND-$(CO_2H)_x$ and THF was sonicated under argon for 5 min. After this time, $LiAlH_4$ was added, and the system was refluxed for 24 h. The reaction mixture was cooled to room temperature and quenched with deionized H_2O. The supernatant liquid was removed by centrifugation at 900 rpm, and the residue was rinsed with deionized H_2O three times. The residue was then heated in 6 M NaOH at 90 ℃ overnight. The reaction mixture was cooled to room temperature, washed, and treated with 0.1 M HCl as described earlier. The repeatedly-washed ND-$(CH_2OH)_n$ **(3)** was dried under vacuum at 50 ^oC. To the ND-$(CH_2ONa)_n$ mixture generated from **(3)** and NaH in THF was added 6-(chloro-hexyloxy)-tetrahydropyran, and the mixture was stirred at 45 ℃ for 24 h. The reaction mixture was cooled to room temperature, washed with THF and water as before, and finally dried under a vacuum. A suspension of ND-$(CH_2O(CH_2)_6OTHP)_x$ **(4)** in MeOH/H_2O (3:1) was sonicated for 5 min; *p*-TsOH was then added until the solution became acidic, after which it was stirred at room temperature overnight. The reaction mixture was worked-up as described earlier to generate **(5)** as a dry powder. Triethylamine was added to a slurry of ND-$(CH_2O(CH_2)_6OH)_x$ **(5)** in THF at 0 ℃, and the mixture was stirred under argon for 30 min. Methanesulfonyl chloride was then added dropwise, and the resulting mixture was stirred at 0 ℃ for 1 h and at room temperature

overnight. Deionized H_2O was added, and the centrifuged residue was washed repeatedly with THF, water, and finally dried under a vacuum to yield ND-$(CH_2O(CH_2)_6OMs)_x$ **(6)**. ND-$(CH_2O(CH_2)_6OMs)_x$ **(6)** was suspended in DMF and sonicated under argon for 5 min; NH_4OH was then added and the mixture was again sonicated for 3 min. It was then stirred at 70 ℃ for 12 h. The reaction mixture was cooled to room temperature and rinsed with THF three times and deionized H_2O twice. Separation by centrifugation at 900 rpm yielded ND-$(CH_2O(CH_2)_6NH_2)_x$ **(7)**, which was then dried under a vacuum. Paclitaxel-2′-succinate **(8)** was prepared according to the known procedure (Zakharian et al., 2005). EEDQ was added to a solution of paclitaxel-2'-succinate **(8)** in dry CH_2Cl_2 and stirred for 30 min at room temperature. To this was added an ultrasonicated suspension of **(7)** and Et_3N in CH_2Cl_2. The resulting mixture was sonicated for an additional 5 min and stirred at room temperature for 3 h. Paclitaxel-conjugated ND **(9)** was separated by centrifugation at 900 rpm and then rinsed three times with CH_2Cl_2, three times with THF, and twice with deionized H_2O; the system was then separated by centrifugation at 900 rpm. The resulting pellet was transferred to a round flask using a small amount of deionized H_2O and dried under a vacuum to give paclitaxel-conjugated ND **(9)** as a dry grey powder. The basic hydrolysis of **(9)** was performed by treating with a 1M solution of sodium hydroxide, sonicating for 5 min,

and stirring overnight at room temperature. The Paclitaxel-hydrolyzed-ND **(10)** thus obtained was separated by centrifugation at 900 rpm, rinsed with THF three times and deionized H_2O twice, and dried under a vacuum.

2.5 Cytotoxicity assay

In all experiments, the powders of ND or ND-paclitaxel were prepared with sterilized distillated water in laminar flow. To avoid aggregation, the samples were ultrasonicated for 20 min at room temperature before use. The MTT systematic name is 3-(4,5-dimethyl-thiazol-2-yl) 2,5-diphenyl tetrazolium bromide, that is agent of offer cell toxicity test. The surviving cells were converted MTT to formazan that generates a blue-purple colour. Briefly, the cells were plated in 96-well plates at a density of 1×10^4 cells/well for 16–20 h. Then the cells were treated with ND or ND-paclitaxel in complete medium for 48 h. Subsequently, the medium was replaced and the cells were incubated with 0.5 mg/ml of MTT in complete medium for 4 h. After 4 h discard supernatant MTT then replaced DMSO. The intensity was measured at 565 nm using a plate reader. The cell viability was calculated by dividing the absorbance of the treated cells by that of the untreated cells.

2.6 Fluorescence intensity of ND-paclitaxel in cells by flow cytometer

The cells were plated at a density of 7×10^5 cells per 60-mm Petri dish in

complete medium for 16-20 h. After treatment with or without ND-paclitaxel, the cells were collected and fixed with ice-cold 70% ethanol overnight at -20℃. The samples were analyzed by flow cytometer. A minimum of ten-thousand cells were analyzed. The fluorescence from the ND-paclitaxel was excited with wavelength 488 nm and the emission was collected in the green light signal range. The fluorescence intensity was quantified by a CellQuest software (BD Biosciences, San Jose, Cal.).

2.7 Confocal microscopy

The cells were cultured on coverslips and kept in a 35-mm Petri dish for 16-20 h before treatment. After treatment with or without ND, ND-paclitaxel, or paclitaxel, the cells were washed with isotonic PBS (pH 7.4) and then were fixed with 4% paraformaldehyde solution in PBS for 1 h at 37℃. Thereafter, the coverslips were washed three times with PBS, and non-specific binding sites were blocked with PBS that contained 10% FBS and 0.25% Triton X-100 for 1 h. The nuclei and β-tubulin were stained with Hoechst 33258 and the Cy3-labeled anti-β-tubulin, respectively. At the end of staining, the samples were examined under a confocal laser scanning microscope (Leica TCS SP2, Mannheim, Baden-Württemberg). The fluorescence images were displayed using the frames stored in the computer, and the images were merged by software written for the Leica confocal microscope (Ver. Lite).

2.8 Cell cycle analysis

To investigate the effect of ND and ND-paclitaxel on the cell cycle progression. The cells were plated at a density of 7×10^5 cells per 60-mm Petri dish in complete medium for 16-20 h. After drug treatment, the cells were collected and fixed with ice-cold 70% ethanol overnight at -20 ℃. Thereafter, the cell pellets were treated with 4 μg/mL propidium iodide solution containing 1% Triton X-100 and 100 μg/mL RNase for 30 min. To avoid cell aggregation, the cell solutions were filtered through a nylon mesh membrane. A minimum of ten thousand cells in each samples were analyzed by CellQuest software in flow cytometer (BD Biosciences, San Jose, Cal.). The percentage of cell cycle phases was quantified by ModFit LT software (Ver. 2.0 and Ver. 3.2, Becton-Dickinson)

2.9 Mitotic index analysis

To determine whether G_2 or M phases increased by ND-paclitaxel, the cells were analyzed by mitotic index. The mitotic cells showed round-up morphology, compact chromosomes, spindle formation, and contained a complete cell membrane but did not produce the cell membrane blebbing or the formation of apoptotic bodies. The adherent cells were cultured on coverslips in a 60-mm Petri dish for 16-20 h before treatment. After treatment, the cells were carefully and gently washed with PBS (pH 7.4) to avoid the loss of mitotically round-up cells, and then fixed with 4%

paraformaldehyde solution in PBS for one hour at 37 ℃. The β-tubulin was stained with the Cy3-labeled mouse anti-β-tubulin (1:50) for 30 min at 37 ℃. Finally, the nuclei were stained with 2.5 μg/mL Hoechst 33258 for 30 min. Mitotic index indicated the percentage of mitotic cell number/total counted cells that was counted under a fluorescence microscope (Leica TCS SP2, Mannheim, Baden-Württemberg) in each treatment.

2.10 Apoptotic nuclear counting

After treatment with or without ND-paclitaxel, the cells were carefully and gently washed with isotonic PBS (pH 7.4), and fixed with 4% paraformaldehyde solution in PBS for one hour at 37 ℃. The β-tubulin was stained with the Cy3-labeled mouse anti-β-tubulin (1:50) for 30 min at 37 ℃. The nuclei were stained with 2.5 μg/mL Hoechst 33258 for 30 min. The number of apoptotic nuclei was counted under a fluorescence microscope (Leica TCS SP2, Mannheim, Baden-Württemberg). The cell morphology of apoptosis was confirmed by the observation of nuclear fragmentation, cell membrane blebbing, and cytoskeleton disruption. The apoptotic percentage (the apoptotic cell number/total counted cells × 100%) was counted under a fluorescence microscope (Leica TCS SP2) in each treatment.

2.11 Annexin V-PI staining

Theapoptosis induction by ND-paclitaxel was analyzed by Annexin V-propidium iodide (PI) assays. The cells were plated in P60 dish at a density of 7 × 10^5 cells/well for 16–20 h. Then the cells were treated with or without ND-paclitaxel in complete medium for 48 h. Then the cells were collected by centrifugation at 1500 rpm. Thereafter, the cells were resuspended in 500 μl of 1X binding buffer and then add 5 μl of Annexin V-FITC and 50 μg/mL PI. Finally, the samples were incubated at room temperature for 5 min in the dark and analyzed by flow cytometer. The cells shows Annexin V^+/PI^- indicated at the early stage apoptosis. The Annexin V^+/PI^+ indicated the late stage apoptosis. The percentage of Annexin V-PI staining cells was quantified from a minimum of 10,000 cells by CellQuest software (BD Biosciences, San Jose, Cal.).

2.12 Time-lapse observation of apoptosis induction

The cells were plated in a 35-nm Petri dish for 16-20 h, then treatment with 1 μg/mL ND-paclitaxel. Immediately, using has the live cell imaging system microscope in long-duration observation for 24 h (OLYMPUS IX71, Japan). The pictures were edited by DP manager software (Ver. 3.3.1, OLYMPUS)

2.13 Western blot analysis

At the end of treatment, the cells were lysed in the ice-cold whole cell extract buffer containing the protease inhibitors. Equal amounts of proteins in samples were

subjected to electrophoresis using sodium dodecyl sulfate-polyacrylamide gels. After electrophoretic, the proteins transfer onto polyvinylidene fluoride membranes (Millipore, Anaheim, Cal.). Then, they were sequentially hybridized with primary antibody and followed with a horseradish peroxidase-conjugated secondary antibody. Finally, the protein bands were visualized using the enhanced chemiluminescence detection system (PerkinElmer Life Sciences, Waltham, MA).

2.14 Xenograft animal model

Lung carcinoma xenograft was developed in 4-6 week-old CB17/Icr-*Prkdc*^{scid}/Crl mice that were obtained from BioLASCO (BioLASCO Co., Ltd., Taipei, Taiwan). The A549 cells were treated with or vehicle, ND, and ND-paclitaxel (10 μg/mL for 48 h). The A549 cells were collected, each mouse was s.c. injection of 1×10^6 cells in 100 μl PBS into the right flank area. The tumor sizes in SCID mice were measured by a digital caliper every four days and calculated tumor volume by the following formula: (length) × (width)^2 × 0.5. Finally, the visible lung tumors were separated from sacrificed xenograft mice.

2.15 Statistical analysis

Each experiment was repeated at least three times. The data were analyzed using t-test, and a p value of < 0.05 was considered as statistically significant in the experiments.

3. Results

3.1 ND-paclitaxel reduces cell viability in lung carcinoma cells

The cell viability of ND, ND-paclitaxel, and NaOH-treated ND-paclitaxel on the A549 human lung carcinoma cells were analyzed by MTT assay. Fig. 1A shows that treatment with 0.1-50 μg/mL ND particles for 48 h did not significantly induce the cytotoxicity of A549 cells. However, ND-paclitaxel for A549 cells cytotoxicity, fig. 1B shows that treatment with ND-paclitaxel for 48 h significantly reduced the cell viability and in a concentration-dependent manner. To further prove the biological activity of paclitaxel on ND, ND-paclitaxel was treated with strong alkaline solution (1 M NaOH), which caused dysfunction of paclitaxel. Indeed, denatured ND-paclitaxel lost the activity to cause the lung cancer cell death (Fig. 1C).

3.2 Uptake ability of ND-paclitaxel in lung carcinoma cells

To analyze the uptake ability of ND-paclitaxel, the cells were analyzed by flow cytometer. Fig. 2A shows that treatment with ND-paclitaxel (0.1-50 μg/mL for 48 h) increased the green fluorescence intensities that the spectra were shifted to right in A549 cells. The quantified fluorescence intensities showed the uptake ability of ND-paclitaxel via a concentration-dependent manner in A549 cells (Fig. 2B). The fluorescence intensities were increased to 4-5-folds in A549 cells than untreated cells at treatment with 50 μg/mL ND-paclitaxel (Fig. 2B).

3.3 ND-paclitaxel blocks microtubules to induce abnormal mitotic cells

To examine whether ND-paclitaxel disturbed microtubule dynamics, A549 cells were treated with ND-paclitaxel and subjected to cytoskeleton and nuclear staining. The green fluorescence from the ND particles was excited by a wavelength of 488 nm and the emission was collected in the range 510-530 nm, the red color was indicated the location of microtubules, and blue color was represented the location of nuclei in A549 cells. Treatment with ND-paclitaxel or paclitaxel markedly increased the abnormal mitotic cell number (Fig. 3A, stars). Fig. 3B shows that treatment with ND-paclitaxel or paclitaxel blocked spindle formation and chromosomes segregation in A549 cells. The disturbance of chromosomes was elicited by ND-paclitaxel or paclitaxel (Fig. 3B, arrows). In contrast, ND particles did not induce the aberrant chromosomes in the A549 cells. Fig. 4A shows that ND-paclitaxel particles were located on the microtubules and blocked the spindle formation. Nevertheless, NaOH-treated ND-paclitaxel particles did not block microtubules and located in cytoplasm by dissection of confocal scanning of Z-axis (Fig. 4B).

3.4 ND-paclitaxel induces the cell cycle arrest and apoptosis in lung carcinoma cells

To investigate the effect of ND-paclitaxel on the cell cycle progression, A549 cells were treated with ND-paclitaxel and analyzed by flow cytometer and mitotic

index. Comparing with untreated and ND-treated samples, ND-paclitaxel dramatically decreased the G_1/G_0 fractions and increased the G_2/M fractions in A549 cells (**$p < 0.01$) (Fig. 5A). The average percentages of G_2/M fractions were elevated at 83.4% after treatment with ND-paclitaxel. In untreated and ND treated samples, the cells were dividing into two daughter cells during cytokinesis; however, ND-paclitaxel blocked cell division and arrested in the prophase of mitosis (Fig. 5B). Furthermore, treatment with 0.1-50 μg/mL ND-paclitaxel for 48 h decreased the mitosis-regulated protein levels of CDC2 and phospho-CDC2 via a concentration-dependent manner in A549 cells (Fig. 6). Actin protein was as an internal control protein, which was not altered by ND-paclitaxel. Additionally, the mitotic index was increased by treated with ND-paclitaxel but not in the untreated, ND alone, and NaOH-treated ND-paclitaxel samples (Fig. 7A).

ND-paclitaxel also significantly increased the sub-G_1 fractions (apoptosis fractions) at the average value of 13.4% in A549 cells, but the sub-G_1 fractions of untreated or ND alone were at the basal level of 2-4% ($p < 0.01$) (Fig. 5A). Besides, we have confirmed and counted the percentage of apoptotic nuclear number by morphological changes under a fluorescence microscope. Consistently, ND-paclitaxel significantly elevated ~12% apoptosis in A549 cells; in contrast, the NaOH-treated ND-paclitaxel lost the ability to increase the apoptosis level (Fig.

7B).

3.5 ND-paclitaxel inhibits tumorigenesis of human lung tumor xenograft in SCID mice

The model of xenograft lung tumor in SCID mice was used to study the effect of ND-paclitaxel on anti-tumorigenesis. The xenograft tumor was developed in five-week-old SCID mice. After treatment with vehicle, ND, or ND-paclitaxel in A549 cells, then cells were collected and mice received 1×10^6 cells by subcutaneously injected. The visible lung tumors that were separated from sacrificed xenograft SCID mice (Fig. 8A). The tumors of mice were growth to average 300–400 mm^3 in control and ND groups after inoculation for 70 days. Moreover, ND-paclitaxel dramatically reduced the tumor size at an average of ~25 mm^3 (Fig. 8B). ND alone did not significantly alter the tumorigenesis of A549 cells in mice during 70 days observation.

3.6 ND-paclitaxel induces cytotoxicity in various human cancer cells

To examine the effect of ND-paclitaxel in other human cancer cells, the colorectal (RKO and HCT116) and bladder (BFTC905) cancer cells were exposed to ND-paclitaxel and analyzed by MTT assay. Fig. 9 shows that treatment with 0.1-50 μg/mL ND-paclitaxel for 48 h significantly reduced the cell viability in all cancer cell types. Furthermore, we found that ND-paclitaxel was more sensitive on

cell death in RKO cells than other cancer cell lines.

3.7 Uptake ability of ND-paclitaxel in colon carcinoma cells

The uptake ability of ND-paclitaxel in RKO cells was examined by flow cytometer. Treatment with ND-paclitaxel (0.1-1 μg/mL for 48 h) elevated the green fluorescence intensities that the spectra were shifted to right in RKO cells (Fig. 10A). The quantified fluorescence intensities showed the uptake ability of ND-paclitaxel (Fig. 10B). The fluorescence intensities were significantly increased by treatment with 0.5-1 μg/mL ND-paclitaxel comparing to untreated cells (Fig. 10B).

3.8 ND-paclitaxel increases sub-G1 and G2/M fractions in colon carcinoma cells

We have examined the effect of ND-paclitaxel on the cell cycle progression and sub-G1 formation in RKO cells. ND-paclitaxel dramatically decreased the G_1/G_0 fractions and increased the G_2/M fractions in RKO cells (Fig. 11A and 11B). ND-paclitaxel also significantly increased the sub-G_1 fractions (apoptosis fractions) in RKO cells (Fig. 11A and 11B). Moreover, ND-paclitaxel decreased the protein levels of CDC2, phospho-CDC2 (Tyr-15 and Thr-161), and cyclin B1 in RKO cells (Fig. 12). The protein level of phosphor-CDC2 (Thr-14) was slightly seduced by ND-paclitaxel. Actin was as an internal control, which was not altered by ND-paclitaxel.

3.9 ND-paclitaxel induces apoptotic formation in colon carcinoma cells

To further examine the effect of ND-paclitaxel apoptosis induction, Annexin V-PI assay was analyzed by flow cytometry. Treatment with 0.5-1 μg/mL ND-paclitaxel for 48 h increased the early and late apoptosis percentage in RKO cells (Fig. 13A). Fig. 13B shows quantified results that treatment with ND-paclitaxel significantly increased the apoptosis. Furthermore, the active forms of caspase-3 were induced following treatment with 0.5-1 μg/mL ND-paclitaxel (Fig. 14). The protein cleavage of PARP, was significantly increased by ND-paclitaxel treatment (Fig. 14). We also confirmed the apoptosis formation following ND-paclitaxel by direct observation of time-lapse cell morphology alteration. Treatment with 1 μg/mL ND-paclitaxel induced apoptosis cells formation (Fig. 15 arrows).

4. Discussion

Chemical drugs linked covalently with nanoparticles have been developed for diagnostic and therapeutic applications in recent years. In this study, we created a novel covalent linkage of ND-paclitaxel. ND-paclitaxel significantly induced the cell death in a variety of cancer cell types. ND-paclitaxel can be taken into lung and colon cancer cells in a concentration-dependent manner. More importantly, ND-paclitaxel exerts its anticancer abilities by inducing mitotic arrest, apoptosis, and anti-tumorigenesis. However, ND alone or denatured ND-paclitaxel did not induce the damage effects on cancer cells. The covalent linkage of nanoparticles and drugs provides the advantage for stabilization to avoid drug dissociation during delivery process. We suggest that ND is a potential nanomaterial for drug delivery and cancer therapy. Recently, it has been demonstrated that carbon nanotubes conjugated with paclitaxel exerted drug delivery for tumor suppression in mice (Liu et al., 2008). Recently, Danhier et. al. reported that paclitaxel-loaded PEGylated PLGA-based nanoparticles displayed greater on the inhibition of tumorigenesis by compared with paclitaxel (Danhier et al., 2009). Moreover, nanoliposomal delivering cancer drugs that have the benefits of prolonged drug in tissue residence during cancer therapy (Chau et al., 2006; Koshkima et al., 2003; Noble et al., 2006). Therefore, nanoparticles provide the opportunities for improving cancer therapeutics by conjugated with cancer drugs.

The toxicity of nanoparticles is a critical issue of concern for clinical applications. Several studies showed that ND did not induce cytotoxicity in various cell types (Liu et al., 2007; Liu et al., 2009; Schrand et al., 2007; Lechleither et al., 2008; Yu et al., 2005; Chang et al., 2008). It is presented that ND particles are non-cytotoxic during cellular division and differentiation (Liu et al., 2009). In the present study, ND particles did not elicit the mitotic blockage and apoptosis in lung cancer cells. Moreover, it is the first time demonstrating that ND particles did not influence the tumorigenesis of human lung cancer cells in xenograft SCID mice. However, ND-paclitaxel is effective to induce the mitotic blockage, apoptosis and anti-tumorigenesis in cancer cells. Recently, it has been reported that no mice showed any symptoms of abnormality after intravenous injection of ND particles (Yuan et al., 2009). We propose that ND is a benign nanomaterial for drug delivery based on its non-cytotoxicity and bio-compatibility.

It has been shown that ND is detectable by its fluorescence property but without photobleaching (Chao et al., 2007; Liu et al., 2009; Yu et al., 2005). We have examined the location and uptake ability of ND-paclitaxel in human carcinoma cells by confocal microscope and flow cytometer. Using confocal microscopy, we observed that ND-paclitaxel was taken into cancer cells and located in the microtubules and cytoplasm. ND particles can be taken into cells by endocytosis pathways such as

clathrin-mediated endocytosis and macropinocytosis (Liu et al., 2009; Faklaris et al., 2008). Interestingly, we found that ND-paclitaxel was uptake into cancer cells in a concentration-dependent manner by flow cytometer analysis. The uptake ability of ND-paclitaxel is correlated to the anticancer activity of paclitaxel on inducing cell death and mitotic blockage in lung cancer cells. ND-paclitaxel has an ester bond between ND and paclitaxel that can be hydrolyzed by esterases. The ester linkage of ND-paclitaxel may be cleaved by esterases of cancer cells for releasing paclitaxel to execute microtubule inhibition and apoptosis. As a whole, the visualization, uptake ability, and paclitaxel released of ND-paclitaxel contain the advantages for cancer drug delivery.

Paclitaxel induced apoptosis pathway through multiple mechanisms (Wang et al., 2000). Moreover, paclitaxel initiated apoptosis has been associated with CDC2 and other CDKs (Donaldson et al., 1994; Meikrantz et al., 1996). In this study, we found that the protein levels of CDC2 and phosphorylated CDC2 (Tyr-15 and Thr161) were decreased by treatment with ND-paclitaxel. We also observed that ND-paclitaxel increased caspase-3 activation and the cleavage of PARP indicating ND-paclitaxel can induce apoptosis pathway in cancer cells. Accordingly, ND-paclitaxel still reserves the anticancer activity of paclitaxel.

5. Conclusion

In summary, we have provided a novel covalent linkage of ND and paclitaxel. More importantly, the covalent bonding of ND-paclitaxel still preserves its anticancer activities on the mitotic blockage, apoptosis induction and anti-tumorigenesis in human lung and colon carcinoma cells. A functional ND-paclitaxel conjugate is potential for drug delivery and cancer therapy.

6. Reference

Akerman, M.E., Chan, W.C., Laakkonen, P., Bhatia, S.N., and Ruoslahti, E. (2002). Nanocrystal targeting in vivo. Proc Natl Acad Sci U S A *99*, 12617-12621.

Alexis, F., Pridgen, E.M., Langer, R., and Farokhzad, O.C. (2010). Nanoparticle technologies for cancer therapy. Handb Exp Pharmacol, *197*, 55-86.

Batist, G., Ramakrishnan, G., Rao, C.S., Chandrasekharan, A., Gutheil, J., Guthrie, T., Shah, P., Khojasteh, A., Nair, M.K., Hoelzer, K., Tkaczuk, K., Park, Y.C., and Lee, L.W. (2001). Reduced cardiotoxicity and preserved antitumor efficacy of liposome-encapsulated doxorubicin and cyclophosphamide compared with conventional doxorubicin and cyclophosphamide in a randomized, multicenter trial of metastatic breast cancer. J Clin Oncol *19*, 1444-1454.

Chang, I.P., Hwang, K.C., and Chiang, C.S. (2008). Preparation of fluorescent magnetic nanodiamonds and cellular imaging. J Am Chem Soc *130*, 15476-15481.

Chou, H.H., Wang, K.L., Chen, C.A., Wei, L.H., Lai, C.H., Hsieh, C.Y., Yang, Y.C., Twu, N.F., Chang, T.C., and Yen, M.S. (2006). Pegylated liposomal doxorubicin (Lipo-Dox) for platinum-resistant or refractory epithelial ovarian carcinoma: a Taiwanese gynecologic oncology group study with long-term follow-up. Gynecol Oncol *101*, 423-8.

Chao, J.I., Perevedentseva, E., Chung, P.H., Liu, K.K., Cheng, C.Y., Chang, C.C., and Cheng, C.L. (2007). Nanometer-sized diamond particle as a probe for biolabeling. Biophys J *93*, 2199-2208.

Cheng, C.L., Chen, C.F., Shaio, W.C., Tsai, D.S., and Chen, K.H. (2005). The CH stretching features on diamonds of different origins. Diamond Relat Mater *14*, 1455–1462.

Cheng, C.Y., Perevedentseva, E., Tu, J.S., Chung, P.H., Chenga, C.L., Liu, K.K., Chao, J.I., Chen, P.H., and Chang, C.C. (2007) Direct and *in vitro* observation of growth hormone receptor molecules in A549 human lung epithelial cells by nanodiamond labeling. Appl Phy Lett *90*, 163903

Danhier, F., Lecouturier, N., Vroman, B., Jerome, C., Marchand-Brynaert, J., Feron, O., and Preat, V. (2009). Paclitaxel-loaded PEGylated PLGA-based nanoparticles: in vitro and in vivo evaluation. J Control Release *133*, 11-7.

Department of health, Executive Yuan, Taiwan (2009). www.doh.gov.tw

Donaldson, K.L., Goolsby, G.L., Kiener, P.A., and Wahl, A.F. (1994). Activation of p34cdc2 coincident with taxol-induced apoptosis. Cell Growth Differ *5*, 1041-1050.

Faklaris, O., Garrot, D., Joshi, V., Druon, F., Boudou, J.P., Sauvage, T., Georges, P., Curmi, P.A., and Treussart, F. (2008). Detection of single photoluminescent

diamond nanoparticles in cells and study of the internalization pathway. Small *4*, 2236-9.

Gao, X., Cui, Y., Levenson, R.M., Chung, L.W., and Nie, S. (2004). In vivo cancer targeting and imaging with semiconductor quantum dots. Nat Biotechnol *22*, 969-976.

Huang, H., Pierstorff, E., Osawa, E., and Ho, D. (2007). Active nanodiamond hydrogels for chemotherapeutic delivery. Nano Lett *7*, 3305-3314.

Huang, L.C., and Chang, H.C. (2004). Adsorption and immobilization of cytochrome c on nanodiamonds. Langmuir *20*, 5879-5884.

Kang, J.H., Asami, Y., Murata, M., Kitazaki, H., Sadanaga, N., Tokunaga, E., Shiotani, S., Okada, S., Maehara, Y., Niidome, T., Hashizume, M., Mori, T., and Katayama, Y. (2010). Gold nanoparticle-based colorimetric assay for cancer diagnosis. Biosens Bioelectron *25*, 1869-1874.

Koshkina, N.V., Waldrep, J.C., and Knight, V. (2003). Camptothecins and lung cancer: improved delivery systems by aerosol. Curr Cancer Drug Targets *3*, 251-64.

Krueger, A. (2008). New Carbon Materials: Biological Applications of Functionalized Nanodiamond Materials. Chem Eur J *14*, 1382-1390

Krueger, A., Stegk, J., Liang, Y., Lu, L., and Jarre, G. (2008). Biotinylated nanodiamond: simple and efficient functionalization of detonation diamond.

Langmuir *24*, 4200-4.

Lechleitner, T., Klauser, F., Seppi, T., Lechner, J., Jennings, P., Perco, P., Mayer, B., Steinmuller-Nethl, D., Preiner, J., Hinterdorfer, P., Hermann, M., Bertel, E., Pfaller, K., and Pfaller, W. (2008). The surface properties of nanocrystalline diamond and nanoparticulate diamond powder and their suitability as cell growth support surfaces. Biomaterials *29*, 4275-4284.

Liu, K.K., Cheng, C.L., Chang, C.C., and Chao, J.I. (2007). Biocompatible and detectable carboxylated nanodiamond on human cell. Nanotechnology *18*, 325102.

Liu, K.K., Wang, C.C., Cheng, C.L., and Chao, J.I. (2009). Endocytic carboxylated nanodiamond for the labeling and tracking of cell division and differentiation in cancer and stem cells. Biomaterials *30*, 4249-4259.

Liu, Z., Chen, K., Davis, C., Sherlock, S., Cao, Q., Chen, X., and Dai, H. (2008). Drug delivery with carbon nanotubes for in vivo cancer treatment. Cancer Res *68*, 6652-6660.

Liu, K.K., Chen, M.F., Chen, P.Y., Lee, T.J.F., Cheng, C.L., Chang, C.C., Ho, Y.P., and Chao, J.I. (2008). Alpha-bungarotoxin binding to target cell in a developing visual system by carboxylated nanodiamond. Nanotechnology *19*, 205102

McNeil, S.E. (2005). Nanotechnology for the biologist. J Leukoc Biol *78*, 585-594.

Meikrantz, W., and Schlegel, R. (1996). Suppression of apoptosis by dominant negative mutants of cyclin-dependent protein kinases. J Biol Chem *271*, 10205-10209.

Michalet, X., Pinaud, F.F., Bentolila, L.A., Tsay, J.M., Doose, S., Li, J.J., Sundaresan, G., Wu, A.M., Gambhir, S.S., and Weiss, S. (2005). Quantum dots for live cells, in vivo imaging, and diagnostics. Science *307*, 538-44.

Nel, A., Xia, T., Madler, L., and Li, N. (2006). Toxic potential of materials at the nanolevel. Science *311*, 622-627.

Noble, C.O., Krauze, M.T., Drummond, D.C., Yamashita, Y., Saito, R., Berger, M.S., Kirpotin, D.B., Bankiewicz, K.S., and Park, J.W. (2006). Novel nanoliposomal CPT-11 infused by convection-enhanced delivery in intracranial tumors: pharmacology and efficacy. Cancer Res *66*, 2801-6.

Schrand, A.M., Huang, H., Carlson, C., Schlager, J.J., Omacr Sawa, E., Hussain, S.M., and Dai, L. (2007). Are Diamond Nanoparticles Cytotoxic? J Phys Chem B Condens Matter Mater Surf Interfaces Biophys *111*, 2-7.

Service, R.F. (2004). Nanotoxicology. Nanotechnology grows up. Science *304*, 1732-1734.

Shimkunas, R.A., Robinson, E., Lam, R., Lu, S., Xu, X., Zhang, X.Q., Huang, H., Osawa, E., and Ho, D. (2009). Nanodiamond-insulin complexes as

pH-dependent protein delivery vehicles. Biomaterials *30*, 5720-8.

Tada, H., Higuchi, H., Wanatabe, T.M., and Ohuchi, N. (2007). In vivo real-time tracking of single quantum dots conjugated with monoclonal anti-HER2 antibody in tumors of mice. Cancer Res *67*, 1138-1144.

Ushizawa, K., Sato, Y., Mitsumori, T., Machinami, T., Ueda, T., and Ando, T. (2002). Covalent immobilization of DNA on diamond and its verification by diffuse reflectance infrared spectroscopy. Chem Phys Lett *351* 105-8.

Wang, T., Lv, J.H., Zhang, X.F., Li, C.J., Han, X., and Sun, Y.J. (2010). Tissue inhibitor of metalloproteinase-1 protects MCF-7 breast cancer cells from paclitaxel-induced apoptosis by decreasing the stability of cyclin B1. Int J Cancer *126*, 362-370.

Wang, T.H., Wang, H.S., and Soong, Y.K. (2000). Paclitaxel-induced cell death: where the cell cycle and apoptosis come together. Cancer *88*, 2619-2628.

Wang, X., Li, J., Wang, Y., Cho, K.J., Kim, G., Gjyrezi, A., Koenig, L., Giannakakou, P., Shin, H.J., Tighiouart, M., Nie, S., Chen, Z., Shin, D.M. (2009). HFT-T, a targeting nanoparticle, enhances specific delivery of paclitaxel to folate receptor-positive tumors. ACS Nano *3*, 3165-3174.

Yang, W., Auciello, O., Butler, J.E., Cai, W., Carlisle, J.A., Gerbi, J.E., Gruen, D.M., Knickerbocker, T., Lasseter, T.L., Russell, J.N., Jr., Smith, L.M., Hamers, R.J.

(2002). DNA-modified nanocrystalline diamond thin-films as stable, biologically active substrates. Nat Mater *1*, 253-257.

Yu, S.J., Kang, M.W., Chang, H.C., Chen, K.M., and Yu, Y.C. (2005). Bright fluorescent nanodiamonds: no photobleaching and low cytotoxicity. J Am Chem Soc *127*, 17604-17605.

Yuan, Y., Chen, Y., Liu, J.H., Wang, H., and Liu, Y. (2009). Biodistribution and fate of nanodiamonds in vivo. Diam Relat Mater *18*, 95-100.

Zhang, B., Li, Y., Fang, C.Y., Chang, C.C., Chen, C.S., Chen, Y.Y., and Chang, H.C. (2009). Receptor-mediated cellular uptake of folate-conjugated fluorescent nanodiamonds: a combined ensemble and single-particle study. Small *5*, 2716-2721.

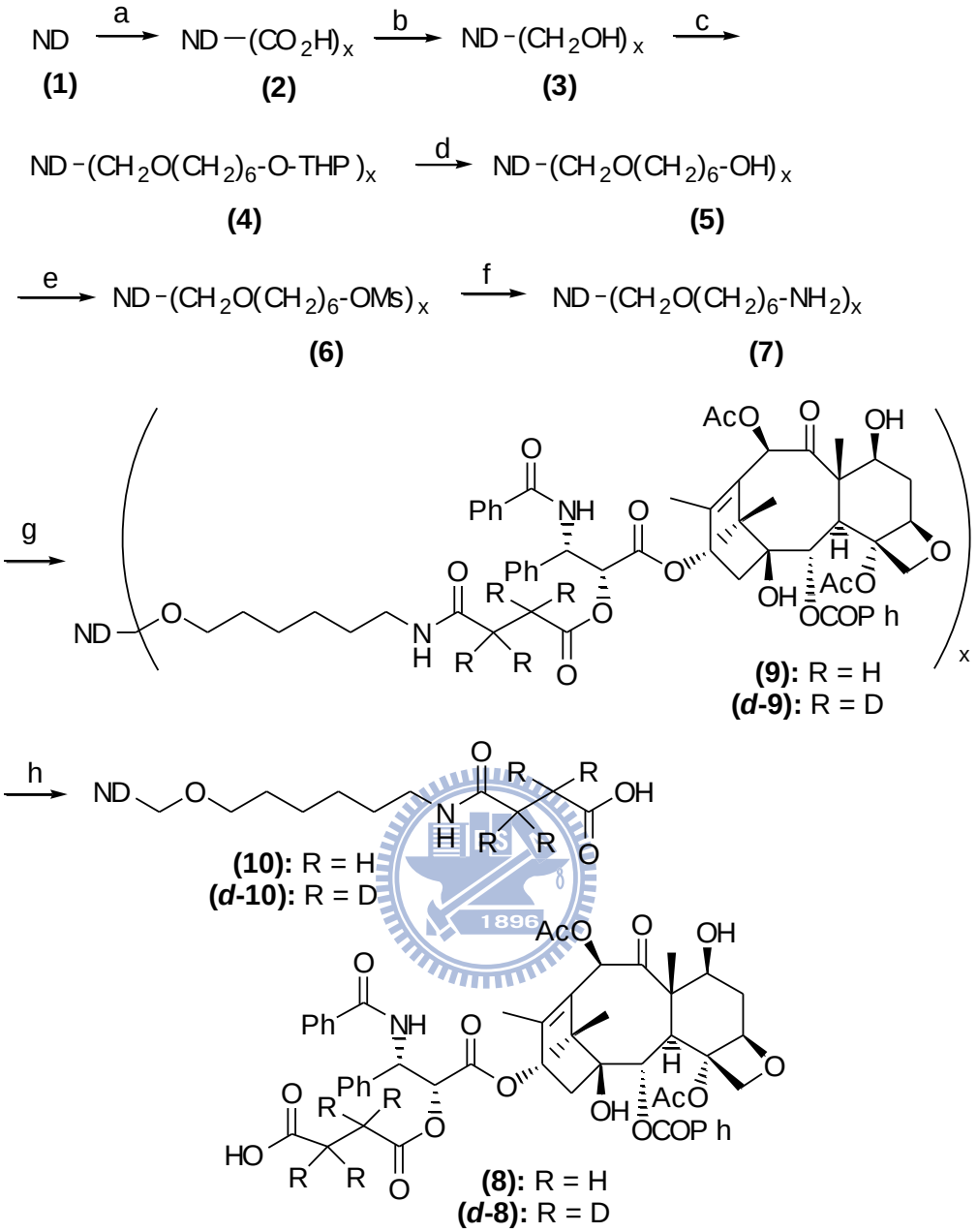

Scheme 1. Chemical synthesis of ND-paclitaxel. The chemical products are indicated by the numbers. The succession of chemical synthetic processes is the following: (a) HCl/HNO_3 (3:1), rt, 3 d; 1M NaOH, 90 ℃, 2 h; 1M HCl, 90 ℃, 2 h; (b) $LiAlH_4$, THF, reflux 24 h; 6M NaOH, 90 ℃, overnight; (c) NaH, THF, THP-O-$(CH_2)_5CH_2Cl$; (d) p-TsOH, $MeOH/H_2O$ (3:1), rt, overnight; (e) MsCl, Et_3N, THF, 0 ℃, 1 h, rt, overnight; (f) NH_4OH(aq), reflux, 24 h; (g) **8** (paclitaxel-2'-succinate), EEDQ, Et_3N, CH_2Cl_2, rt, 3 h; (h) 1M NaOH, rt, overnight.

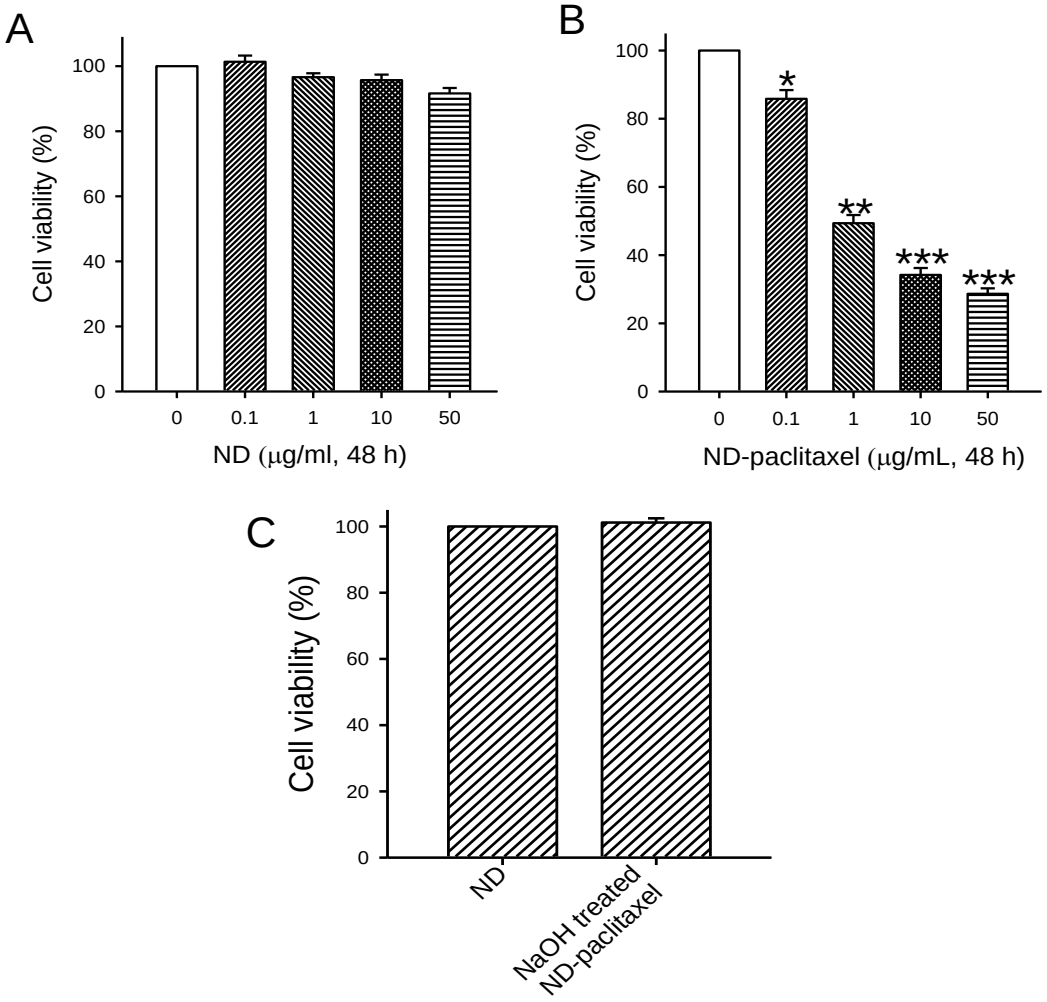

Figure 1. Effect of ND-paclitaxel on the cell viability in human lung carcinoma cells. (A) A549 cells were treated with or without ND (0.1-50 μg/mL for 48 h). (B) A549 cells were treated with or without ND-paclitaxel (0.1-50 μg/mL for 48 h). At the end of treatment, the cell viability was measured by MTT assay. Results were obtained from four-twelve separate experiments and the bar represents mean ± S.E. $^{*}p < 0.05$, $^{**}p < 0.01$, and $^{***}p < 0.001$ indicate significant difference between control and ND-paclitaxel treated samples. (C) A549 cells were treated with 50 μg/mL ND particles or NaOH-treated ND-paclitaxel for 48 h. The cell viability was measured by MTT assay. Results were obtained from eight experiments and the *bar* represents mean ± S.E.

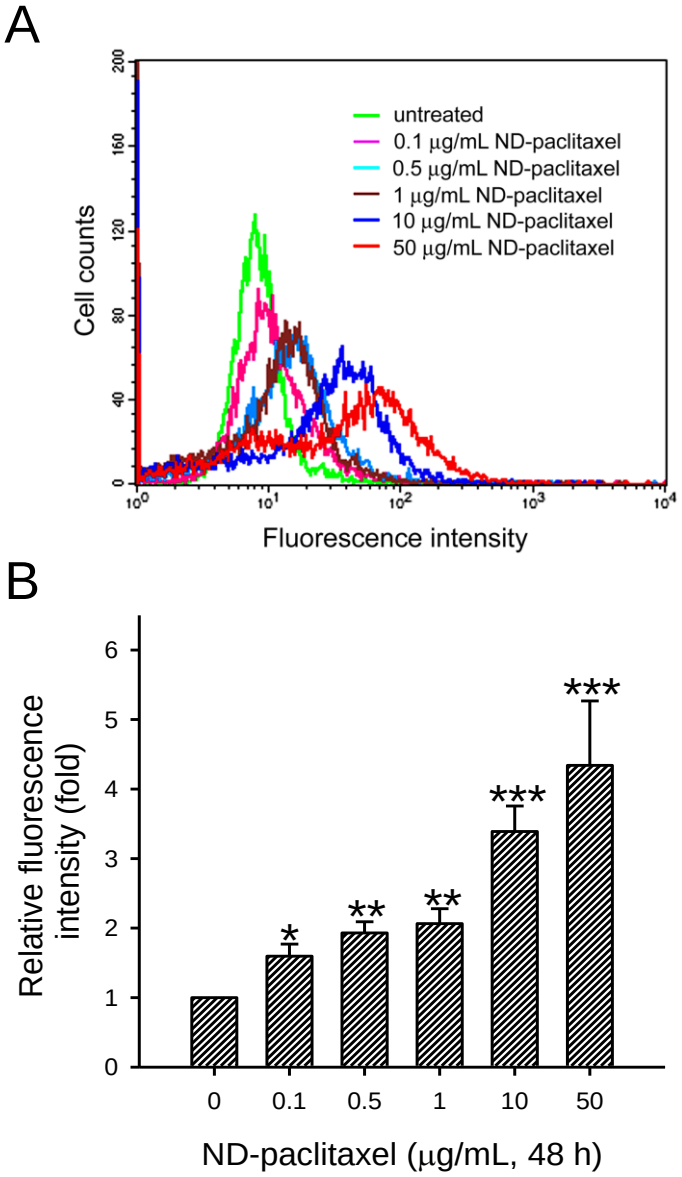

Figure 2. Uptake ability of ND-paclitaxel in human lung carcinoma cells. (A) A549 cells were treated with 0-50 μg/mL ND-paclitaxel for 48 h. At the end of treatment, the cells were trypsinized and then subjected to flow cytometer. (B) The fluorescence intensities were quantified by a CellQuest software of flow cytometer. Results were obtained from four separate experiments and the *bar* represents the mean ± S.E. $^{*}p < 0.05$, $^{**}p < 0.01$, and $^{***}p < 0.001$ indicate significant difference between untreated and ND-paclitaxel samples.

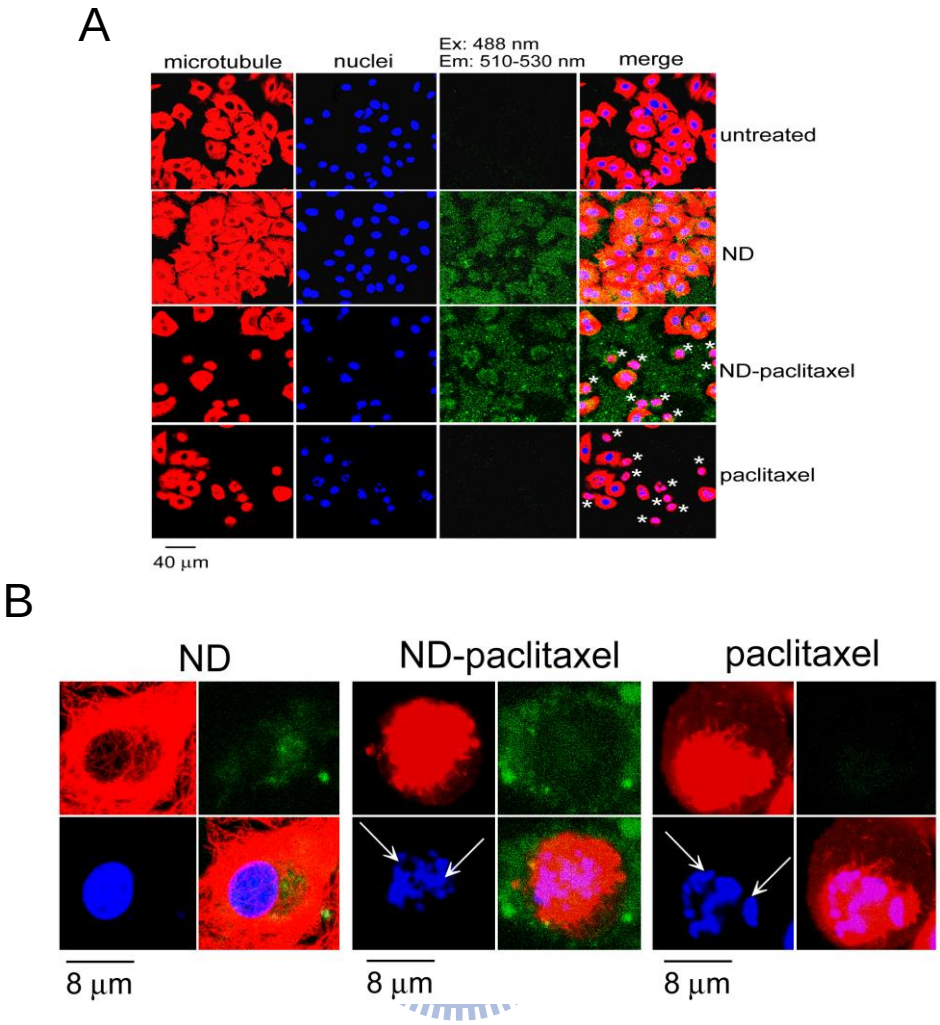

Figure 3. Effect of ND-paclitaxel on the blockage of microtubule and chromosome segregation in human lung carcinoma cells. (A) A549 cells were treated with ND (50 μg/mL), ND-paclitaxel (50 μg/mL), or paclitaxel (50 nM) for 24 h. The microtubule were stained with Cy3-labeled mouse anti-β-tubulin. The nuclei were stained with Hoechst 33258. Microtubules and nuclei were exhibited red and blue color, respectively. The green fluorescence from ND particles was excited by a wavelength of 488 nm and the emission was collected in the range 510-530 nm by using confocal microscope. The stars indicate that the cell morphology (mitotic round-up) was affected by paclitaxel or ND-paclitaxel compared to untreated or ND treated samples. (B) The pictures are amplified from (A). The arrows indicate the derangement of chromosomes after treatment with paclitaxel or ND-paclitaxel.

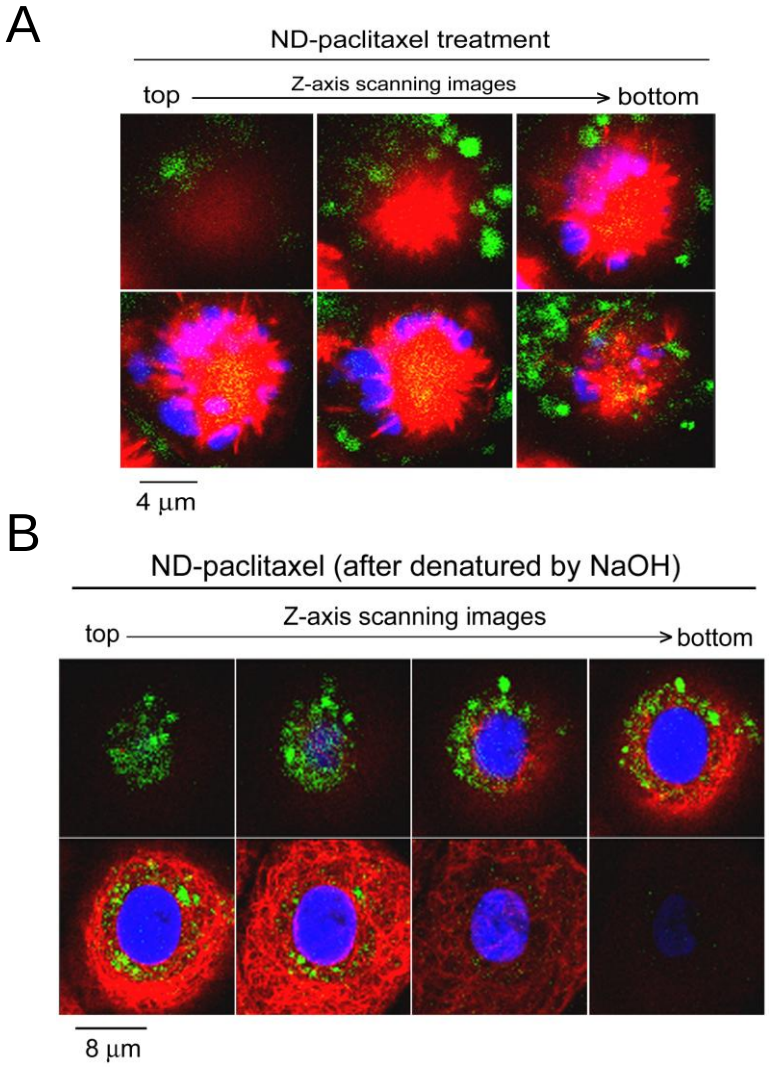

Figure 4. Location and distribution of ND-paclitaxel in human lung carcinoma cells. (A) An A549 cell from ND-paclitaxel (50 μg/mL for 24 h) treatment was visualized by examining Z-axis scanning images using a confocal microscope. The distribution of ND-paclitaxel interacting with microtubules was observed by scanning in the vertical direction from top to bottom. Microtubule and nuclei exhibited red and blue color, respectively. The green color indicates the location of ND particles. The yellow color indicated that ND-paclitaxel particles were co-localized with microtubules. (B) An A549 cell from NaOH-treated ND-paclitaxel (50 μg/mL for 24 h) treatment was visualized by examining Z-axis scanning images of a confocal microscope.

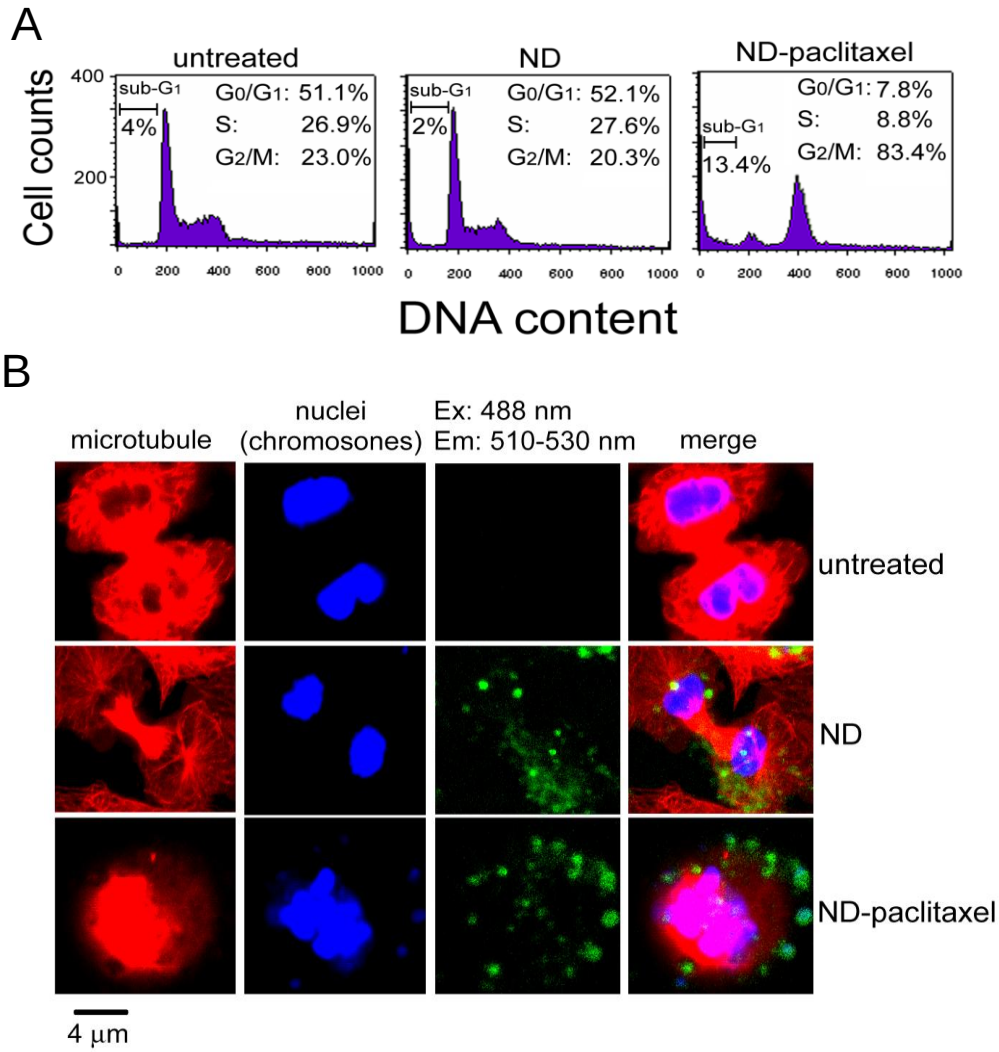

Figure 5. Effect of ND-paclitaxel on the cell cycle progression in human lung carcinoma cells. A549 cells were treated with 50 μg/mL ND or ND-paclitaxel for 24 h. (A) At the end of treatment, the A549 cells were trypsinized and then subjected to flow cytometry analyses. These data of each cell cycle phases and sub-G1 fractions were represented the average values from three separate experiments. (B) The β-tubulin and nuclei were stained with the Cy3-labeled mouse anti-β-tubulin and Hoechst 33258, respectively. Microtubules and nuclei were exhibited red and blue color, respectively. The green fluorescence from ND particles was excited by a wavelength of 488 nm and the emission was collected in the range 510-530 nm by using confocal microscope. The untreated and ND-treated cells were separating to two daughter cells during cytokinesis. The ND-paclitaxel-treated cell was arrested in the prophase of mitosis.

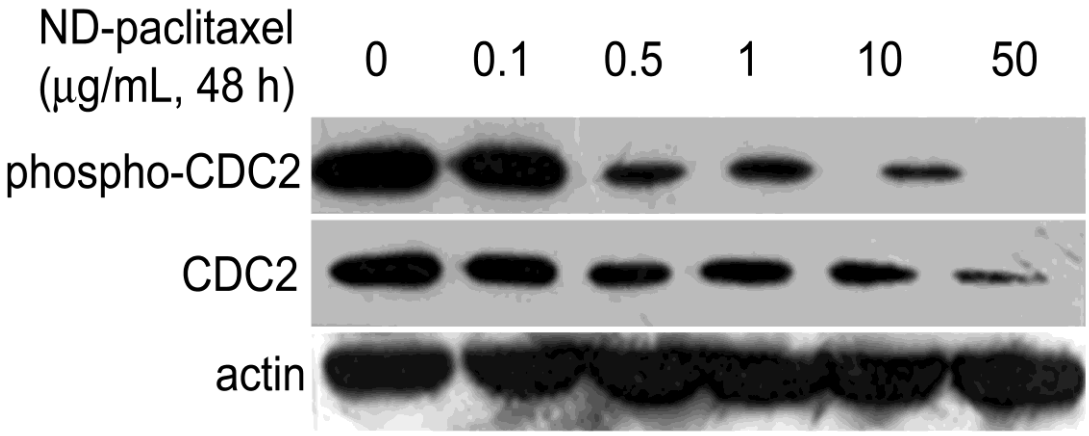

Figure 6. The effect of ND-paclitaxel on the protein levels of phospho-CDC2 and total CDC2 in human lung carcinoma cells. A549 cells were treated with or without ND-paclitaxel (0.1-50 μg/mL for 48 h). The total protein extracts were subjected to Western blot analysis by using anti- phospho-CDC2, anti-CDC2, and actin antibodies. Representative Western blot results were shown from one of three separate experiments with similar findings.

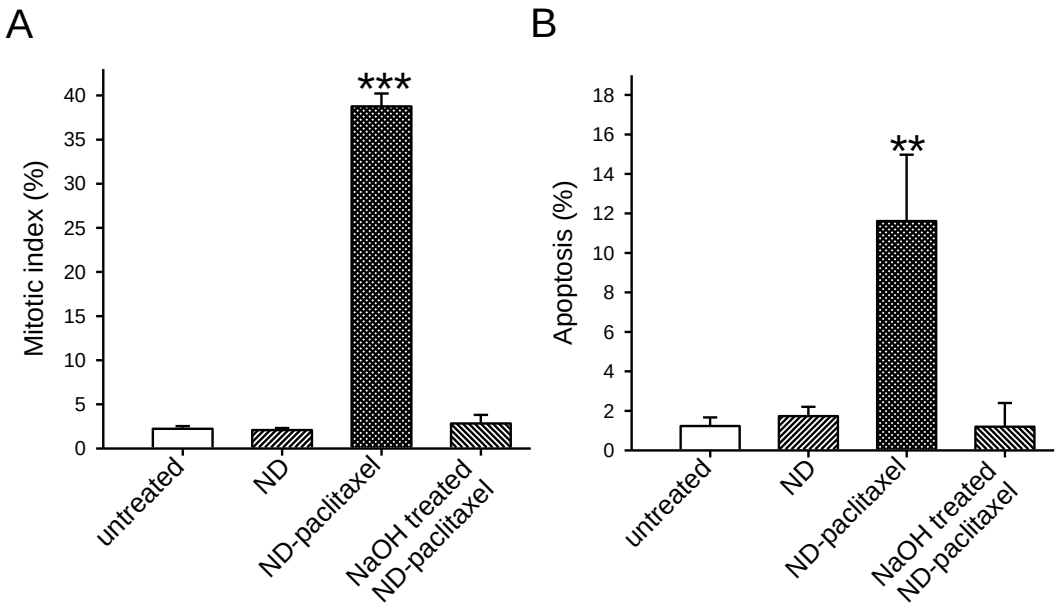

Figure 7. Effect of ND-paclitaxel on the percentages of mitotic index and apoptosis in human lung carcinoma cells. A549 cells were treated with 50 μg/mL ND, ND-paclitaxel, or NaOH-treated ND-paclitaxel for 24 h. (A) After the end of treatment, the β-tubulin and nuclei were stained with the Cy3-labeled mouse anti-β-tubulin and Hoechst 33258, respectively. Mitotic index (the percentage of mitotic cell number/total cell number) was counted under a fluorescence microscope. (B) The percentage of apoptosis was counted by apoptotic nuclei. Results were obtained from three separate experiments and the *bar* represents the mean ± S.E. $^{**}p < 0.01$ and $^{***}p < 0.001$ indicate significant difference between the controls and ND-paclitaxel.

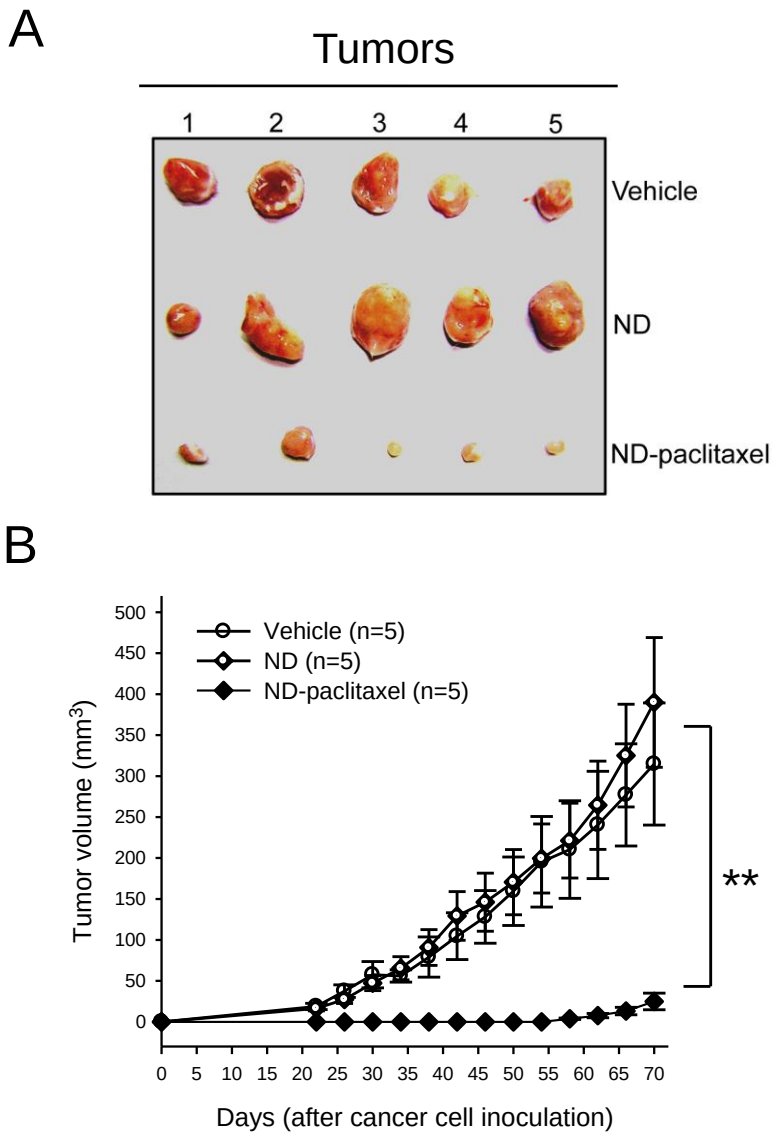

Figure 8. The effect of pretreated ND and ND-paclitaxel on tumor growth in xenograft SCID mice model. (A) A549 cells were treated with ND or ND-paclitaxel (10 mg/mL for 48 h). Then the SCID mice were subcutaneously injected with 1×10^6 cells. The visible lung tumors were separation from sacrificed xenograft mice after inoculation for 70 days. (B) The tumor volume in SCID mice were measured every four days until 70 days. The bar represents the mean ± S.E. **$p < 0.01$ indicates significant difference between the controls and ND-paclitaxel.

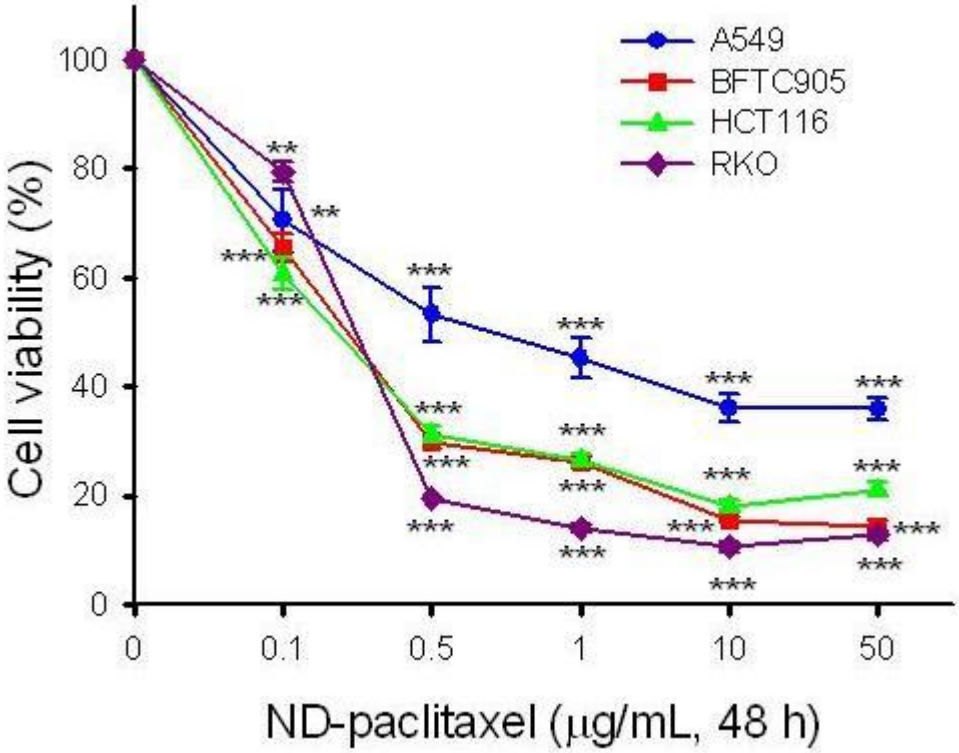

Figure 9. Effect of ND-paclitaxel on the cell viability in various human cancer cells. A variety of cancer cell lines including lung (A549), colorectal (RKO and HCT116), and bladder (BFTC 905) cancer cells were treated with or without ND-paclitaxel (0.1–50 μg/mL for 48 h). The cell viability was measured by MTT assay. The results were from 4-8 separated experiments. The bar represents mean ± S.E. **$p < 0.01$, and ***$p < 0.001$ indicate significant difference between control and ND-paclitaxel treated sample.

A

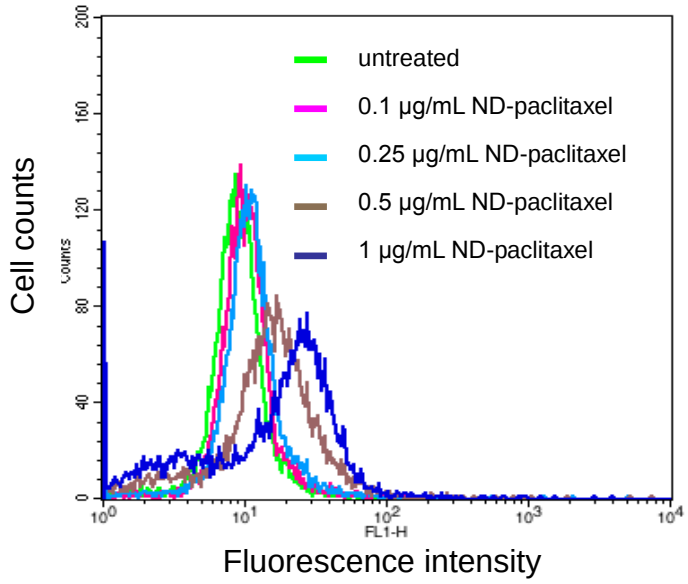

B

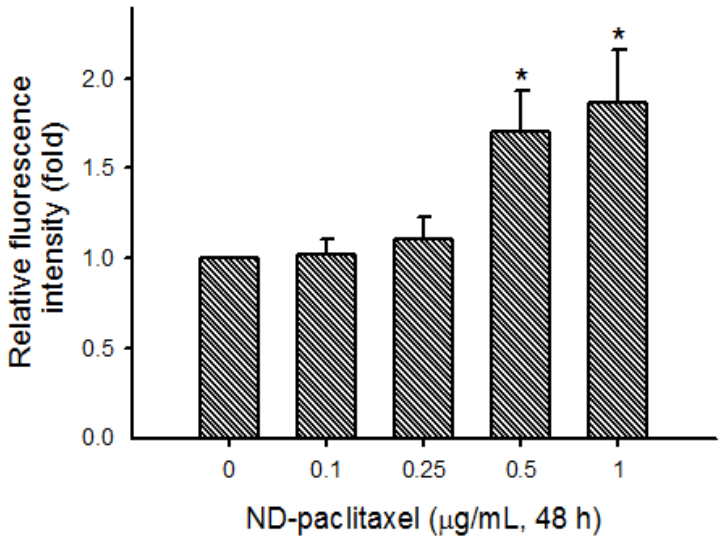

Figure 10. Uptake ability of ND-paclitaxel in human colon cancer cells. (A) RKO cells were treated with 0-1 μg/mL ND-paclitaxel for 48 h. At the end of treatment, the cells were harvested and subjected to flow cytometer. (B) The fluorescence intensities of ND-paclitaxel in RKO cells were quantified by CellQuest software of flow cytometer. Results were obtained from three separate experiments and the bar represents the mean ± S.E. *$p < 0.05$ indicate significant difference between untreated and ND-paclitaxel samples.

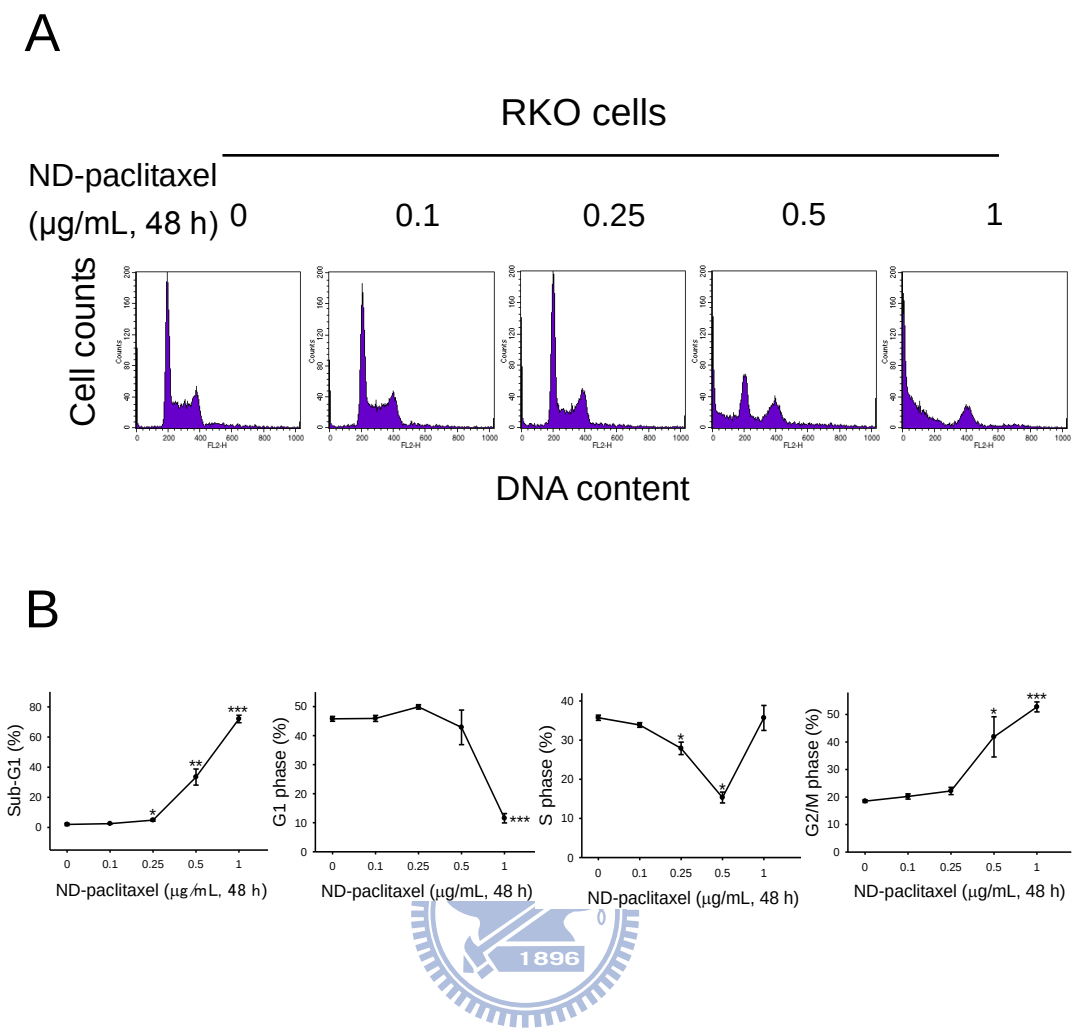

Figure 11. Effect of ND-paclitaxel on cell cycle progression in human colon cancer cells. (A) RKO cells were treated with or without ND-paclitaxel (0.1-1 μg/mL for 48 h). At the end of treatment, the RKO cells were trypsinized and then subjected to flow cytometry analyses. (B) The each cell cycle phases were quantified by ModFit LT software of flow cytometer. Results were obtained from three experiments and the bar represents mean ± S.E. $^{*}p < 0.05$, $^{**}p < 0.01$, and $^{***}p < 0.001$ indicate significant difference between control and ND-paclitaxel treated samples.

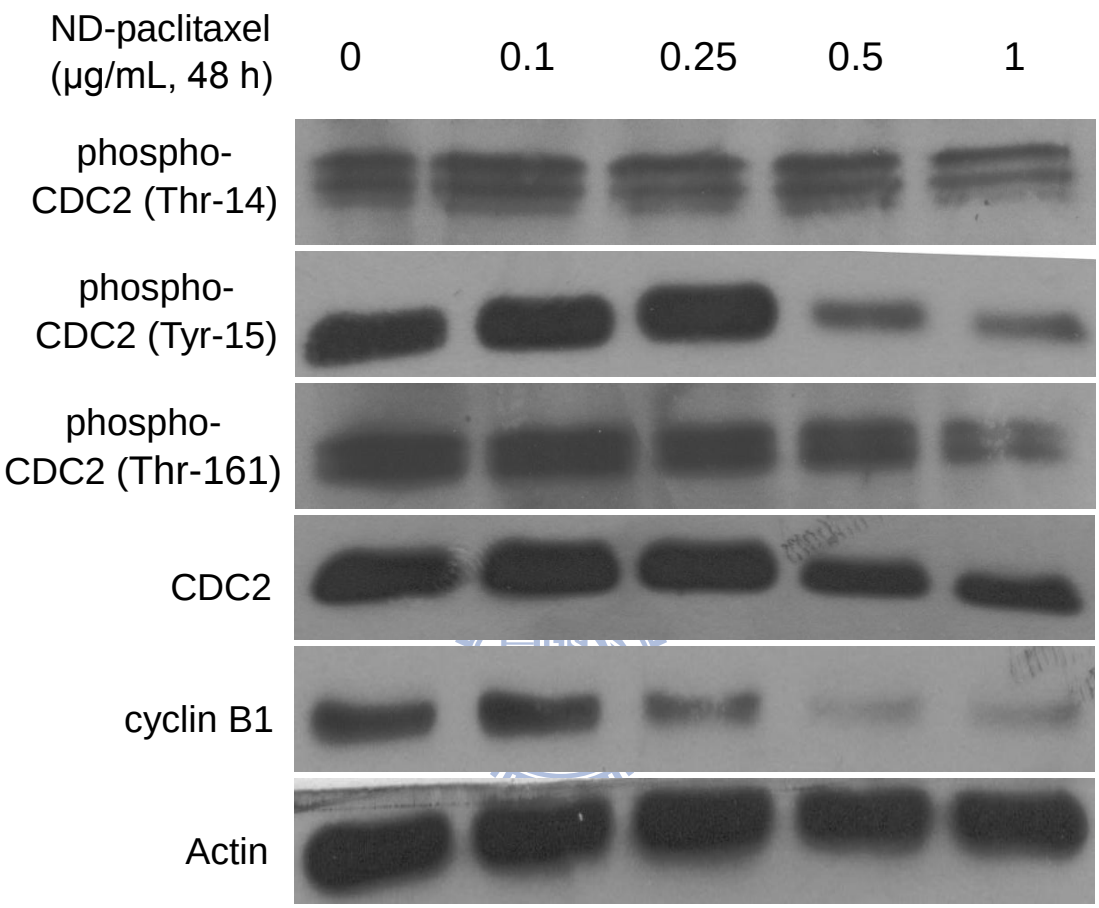

Figure 12. Effect of ND-paclitaxel on the protein levels of phosphorylated CDC2, total CDC2 and cyclin B1 in human colon cancer cells. RKO cells were treated with or without ND-paclitaxel (0.1-1 μg/mL for 48 h), total protein extracts were prepared for Western blot analysis using specific anti-phospho-CDC2 (Thr-14, Tyr-15, and Thr-161), anti-CDC2, anti-cyclin B1 and actin antibodies. Western blot data were shown from one of three separate experiments with similar findings.

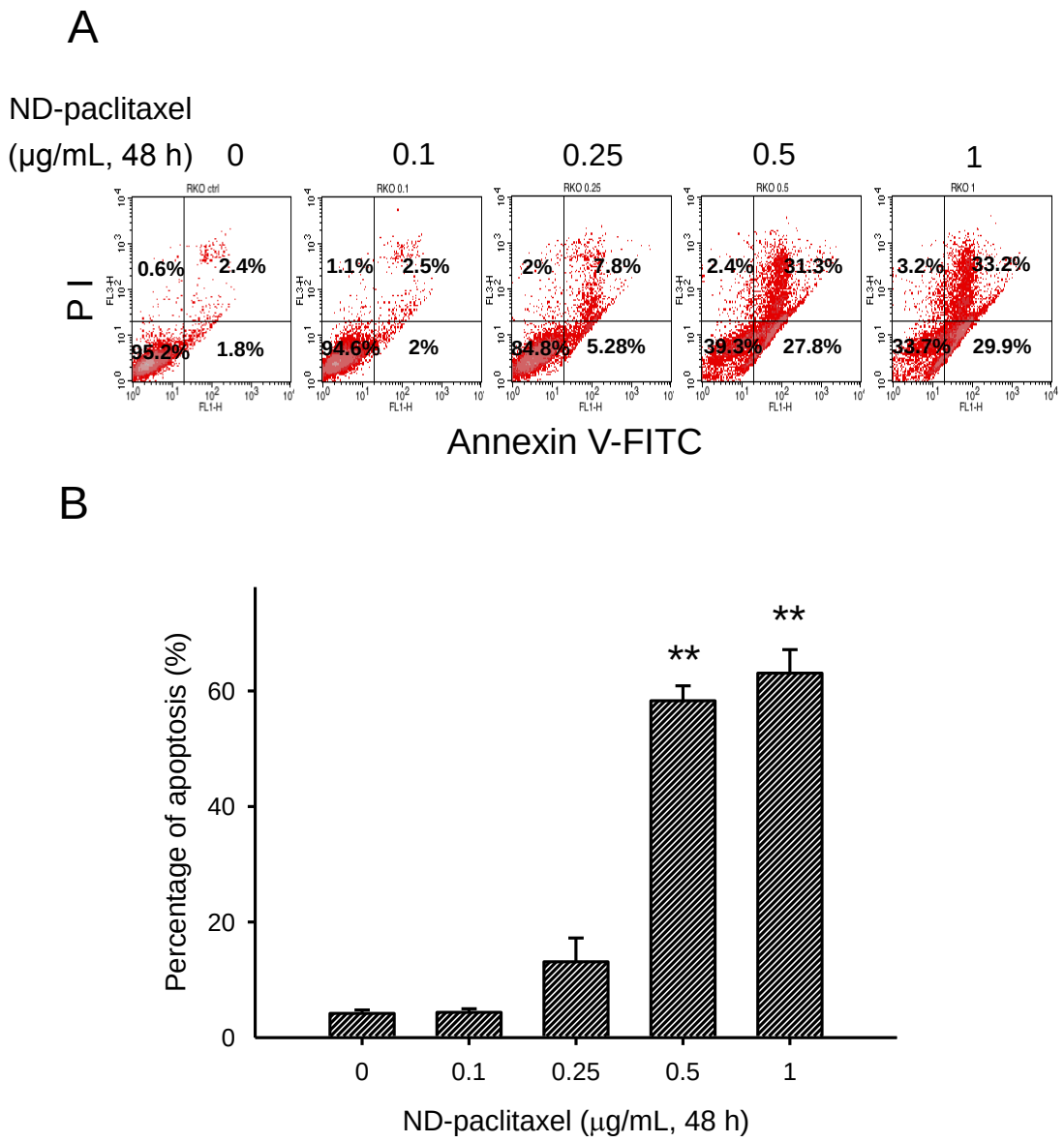

Figure 13. Effect of ND-paclitaxel for apoptosis in the RKO cells. (A) RKO cells were treated with or without 0.1-1 μg/mL ND-paclitaxel for 48 h. At the end of treatment, the A549 cells were trypsinized and then the cells were analyzed by Annexin V-FITC assay. The percentages of the cell forms mentioned below were calculated by the CellQuest software (mean values are given). (B) The early and late apoptosis cells were quantified by CellQuest software of flow cytometer. Results were obtained from three experiments and the *bar* represents the mean ± S.E. $^{**}p < 0.01$ indicate significant difference between untreated and ND-paclitaxel samples.

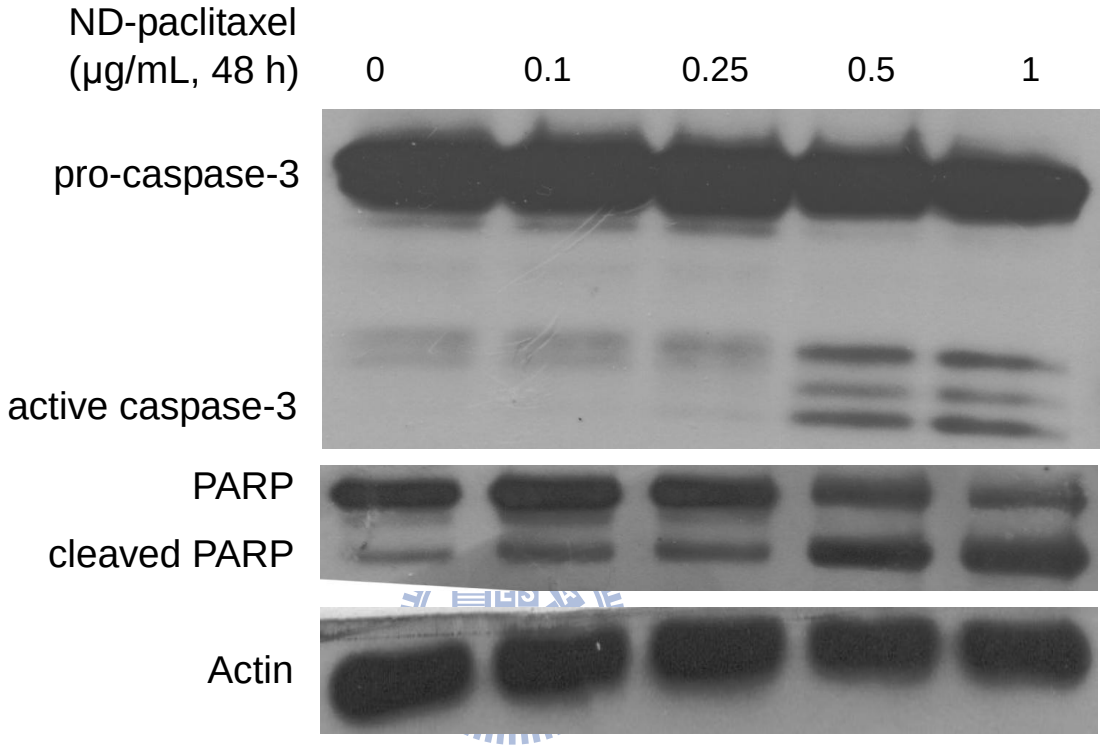

Figure 14. Effect of ND-paclitaxel on the active of caspase-3 and cleavage of poly(ADP-ribose) polymerase (PARP) in human colon cancer cells. Induce of caspase-3 was activated and PARP cleavage by ND-paclitaxel at the indicated concentrations after 48 h of treatment.

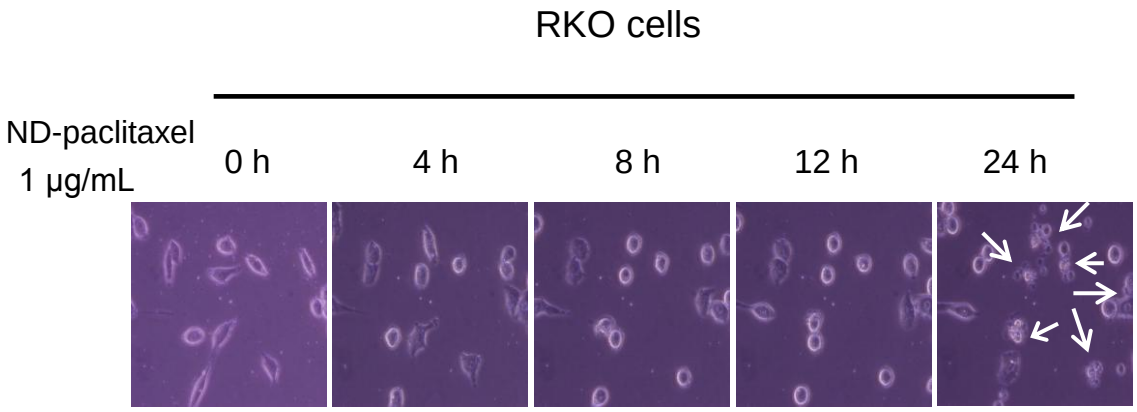

Figure 15. Time-lapse observation of apoptotic formation following treatment with ND-paclitaxel. RKO cells were treated with ND-paclitaxel 1 μg/mL. The cell were immediately observed by live-cell imaging microscope for 0-24 h. The arrows indicate the apoptotic cells by ND-paclitaxel treatment.